Human Molecular Genetics, 2021, Vol. 30, No. 22 2177–2189

https://doi.org/10.1093/hmg/ddab181
Advance Access Publication Date: 6 July 2021
Bioinformatics Article

BIOINFORMATICS ARTICLE

Integrative analysis of genomic and epigenomic data reveal underlying superenhancer-mediated microRNA regulatory network for human bone mineral density

Wei-Yang Bai[1,2,3,4], Jiang-Wei Xia[2,3,4], Xiao-Li Rong[5], Pei-Kuan Cong[2,3,4], Saber Khederzadeh[2,3,4] and Hou-Feng Zheng[1,2,3,4,*]

[1]Fudan University, Shanghai 200433, China, [2]Diseases & Population (DaP) Geninfo Lab, School of Life Sciences, Hangzhou 310024 Zhejiang, China, [3]Westlake Laboratory of Life Sciences and Biomedicine, Hangzhou 310024, Zhejiang, China, [4]Institute of Basic Medical Sciences, Westlake Institute for Advanced Study, Hangzhou 310024, Zhejiang, China and [5]Institute for Cell Engineering, The Johns Hopkins University School of Medicine, Baltimore, MD 21205, USA

*To whom correspondence should be addressed. Email: zhenghoufeng@westlake.edu.cn

Abstract

Bone mineral density (BMD) is a highly heritable complex trait and is a key indicator for diagnosis and treatment for osteoporosis. In the last decade, numerous susceptibility loci for BMD and fracture have been identified by genome-wide association studies (GWAS); however, fine mapping of these loci is challengeable. Here, we proposed a new long-range fine-mapping approach that combined superenhancers (SEs) and microRNAs (miRNAs) data, which were two important factors in control of cell identity and specific differentiation, with the GWAS summary datasets in cell-type-restricted way. Genome-wide SE-based analysis found that the BMD-related variants were significantly enriched in the osteoblast SE regions, indicative of potential long-range effects of such SNPs. With the SNP-mapped SEs (mSEs), 13 accessible long-range mSE-interacted miRNAs (mSE-miRNAs) were identified by integrating osteoblast Hi-C and ATAC-seq data, including three known bone-related miRNAs (miR-132-3p, miR-212-3p and miR-125b-5p). The putative targets of the two newly identified mSE-miRNAs (miR-548aj-3p and miR-190a-3p) were found largely enriched in osteogenic-related pathway and processes, suggesting that these mSE-miRNAs could be functional in the regulation of osteoblast differentiation. Furthermore, we identified 54 genes with the long-range 'mSE-miRNA' approach, and 24 of them were previously reported to be related to skeletal development. Besides, enrichment analysis found that these genes were specifically enriched in the post-transcriptional regulation and bone formation processes. This study provided a new insight into the approach of fine-mapping of GWAS loci. A tool was provided for the genome-wide SE-based analysis and the detection of long-range osteoblast-restricted mSE-miRNAs (https://github.com/Zheng-Lab-Westlake/Osteo-Fine-Mapp-SNP2SE2miRNA).

Introduction

Osteoporosis is a common skeletal disease characterized by reduced bone mass and deterioration in bone microarchitecture, leading to an increased propensity to fragility fracture (1). Bone mineral density (BMD), which is generally evaluated by dual energy X-ray absorptiometry scan (DXA), is a key indicator for diagnosis and treatment for osteoporosis (2). Bone mass could also be estimated by ultrasound approach by considering both the speed of sound and bone ultrasound attenuation. In the last

Received: March 31, 2021. **Revised:** June 17, 2021. **Accepted:** June 29, 2021

decade, genome-wide association studies (GWAS) have identified many susceptible loci for BMD at several anatomical sites such as lumbar spine (LS), femoral neck (FN), forearm (FA) and total body (3–6). In 2018, a GWAS with 426 824 individuals from UK biobank dataset identified 518 genome-wide significant loci associated with heel estimated BMD (eBMD), including 301 novel loci (7). However, it is challengeable to pinpoint susceptible genes from an associated locus, some studies have successfully identified the determinant genes of BMD and fracture, such as *EN1* and *DAAM2* (5,7). The commonly used approach for susceptible gene selection is to identify the lead SNP-overlapped protein coding gene directly or the nearest gene (8). However, the vast majority of associated variants are non-coding, residing at intronic and intergenic regions in genome. Besides that, some variants appear to be in one gene but influencing the expression of others due to the spatial state of chromatin (9). One example is that obesity-associated variants within *FTO* gene form long-range functional connections with *IRX3* (10). Variants reside in some functionally important region, such as enhancers, may affect distant genes by long-range interactions, cell-type-specific Hi-C and ATAC-seq, which could show spatial interactions and the accessibility of chromatin (11,12), might detect these long-range interactions.

Superenhancers (SEs) are large clusters of regulatory regions that consist of multiple enhancers occupied by high density of mediator complexes that drive expression of cell-identity genes (13–15), previous studies found that enhancers within SEs possess stronger activating features than normal enhancers (16–18). SEs are generally enriched for disease-associated variants, especially for the SEs defined in the disease-relevant cell type or tissue (15,19). For example, SEs identified in human pancreatic islet cells are enriched for SNPs associated with type 2 diabetes (20), and Alzheimer's disease-associated SNPs are found to reside in brain tissue SEs (15).

MicroRNAs (miRNAs) are a class of short non-coding RNAs that block protein translation or modulate mRNA stability by specifically binding the complementary sequences in the 3′ untranslated region (UTR) of mRNAs (21). Many miRNAs are found involved in multiple developmental osteogenic signaling pathways and osteoblast growth and differentiation pathways (22–25), such as miR-125b could downregulate cell proliferation and inhibit osteoblastic differentiation (26), and miR-212 and miR-384 could promote osteogenic differentiation via targeting *RUNX2* (27). MiRNAs are transcribed by RNA polymerase (Pol) II/III into primary miRNA (pri-miRNA), which are processed by Drosha/Dgcr8 into precursor miRNA (pre-miRNA) (28).

Interestingly, the tissue-specific miRNA expression atlas was found largely shaped by SEs and H3K4me3 domains, SEs could facilitate transcription, Drosha/Dgcr8 recruitment and pri-miRNA processing to boost cell-type-specific miRNA production (14). In addition, previous studies have found that SEs and miRNAs both play a key role in the control of cell-type-specific transcriptomes (14,29), in view of this, SE-interacted miRNAs (SE-miRNAs) may have some specific properties in the maintenance of cell identity and differentiation. We therefore applied a cell-type-restricted approach that combined SEs and miRNAs for the fine-mapping of GWAS SNPs. In this study, we mapped SEs with BMD-associated SNPs from 10 large-scale human GWAS datasets and identified long-range osteoblast SNP-mapped SE-miRNAs and genes for human BMD and fracture by integrating multiple genomic and epigenomic datasets. Our approach could also be generalized to the other cell-type-specific traits or diseases.

Results

BMD-associated SNP landscape in human osteoblast SEs and genome-wide SE-based analysis

The overall study design was shown in Figure 1. We employed histone modification marker of H3K27ac to shape the enhancer regions in genome in human osteoblast. A total of 72 936 and 116 190 peaks were initially called from two replicates H3K27ac ChIP-seq data, and a total of 1224 and 1149 SEs were detected from the peaks (Supplementary Material, Fig. S1, Supplementary Material, Tables S1 and S2). We next compared them with the human osteoblast SEs from SEA and dbSUPER database, the results showed a high degree of consistency between these SEs (Supplementary Material, Fig. S2). Besides, we also compared our SEs with the human fetal osteoblasts (undifferentiated and differentiated) SEs from SEdb, there were few differences were found, this could be caused by the different osteoblastic cell type used (Supplementary Material, Fig. S2). We extracted SNPs that resided in SEs from 10 large-scale BMD-related GWAS datasets, the landscapes of such SNPs in the genome were shown in Figure 2 and Supplementary Material, Figure S3. We found that many genome-wide significant BMD-associated SNPs were enriched in osteoblast SEs, particularly for heel eBMD and total body DXA BMD (Fig. 2). This result suggested a potential long-range effect of these SNPs via SEs. We then pruned out all non-independent SNPs in the 10 GWAS datasets. The SE-based mapping analysis for two replicates then respectively yielded 202 and 291 SNP-mapped SEs (mSEs) that passed Bonferroni multiple-test, these osteoblast mSEs could be functional important for BMD (Supplementary Material, Tables S3 and S4).

Identification of Long-range mSE-miRNA in human osteoblast

We first defined the promoter bait regions of 1914 pri-miRNAs (Supplementary Material, Table S5). After applying the promoter-focused Hi-C data and overlapping analysis, we found there were 74 pri-miRNAs that had DNA-looping interaction with mSEs (Supplementary Material, Table S6), most of them had at least two Hi-C interactions and a half of mSEs were mapped by 50–90 independent SNPs (Supplementary Material, Figure S4). The SNP signals in these mSEs were mainly from heel ultrasound eBMD GWAS, a few of signals were from total body and other anatomical sites DXA BMD GWAS. Among 74 mSE-miRNAs, 12 of them were previously found to be associated with osteogenic differentiation, and two pri-miRNAs were associated with muscle proliferation (Supplementary Material, Table S7).

We further investigated the chromatin accessibility of the 74 mSE-miRNAs by ATAC-seq data in primary human mesenchymal stem cells (MSCs)-derived osteoblasts (9). Thirteen pri-miRNAs were finally identified that had the open chromatin conservative region in the corresponding promoter or transcriptional start sites (TSS) region, Figure 3 demonstrated the detailed mapping and long-range interactions results. The distributions of H3K27ac peaks on the genome in two biological replicates showed the similar pattern, and the number of long-range interactions and distance between mSE and miRNAs were varied (Fig. 3). Among all mSE-miRNAs, mir-125b-1 (Fig. 3A), mir-548aj-1 (Fig. 3D), mir-614 (Fig. 3F) and mir-5702 (Fig. 3J) were found to have the most DNA-looping interactions with mSE, which respectively reached 0.11, 1.01, 0.56 and 0.3 per kb in mSE, reflecting the high spatial contact density in genome (Table 1); the mir-614 (Fig. 3F) and mir-3650 (Fig. 3H) showed the furthest

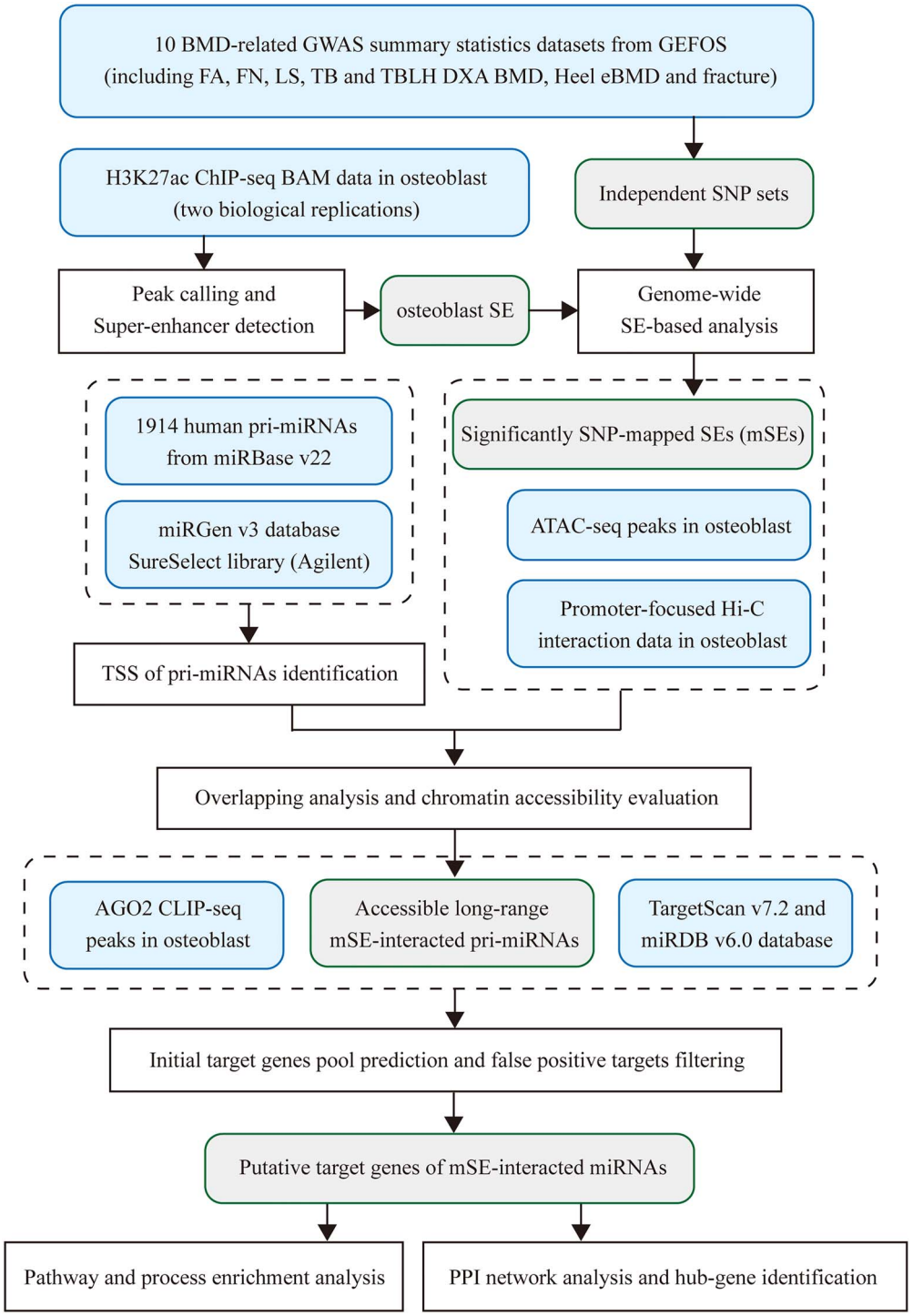

Figure 1. Study design.

distance (>250 kb) with the corresponding mSE, whereas mir-6870 (Fig. 3 L) was found overlapped within mSE; the mir-132 (Fig. 3B), mir-212 (Fig. 3B) and mir-614 (Fig. 3F) were found interacted by two remote mSEs simultaneously. Besides, there were two pri-miRNAs, mir-125b-1 (Fig. 3A, mSE *P*-value: 1.9e−11, best SNP *P*-value: 3.6e−8) and mir-583 (Fig. 3E, mSE *P*-value: 1.7e−17, best SNP *P*-value: 8.6e−14), that were found interacted with the mSEs mapped by intergenic SNPs, indicative of the functional importance of GWAS signals in such regions (Table 1). These accessible mSE-miRNAs could be the vehicles for SNP loci to regulate the expression of genes in osteoblast.

Putative targets of 13 accessible mSE-miRNAs and biological process enrichment

We predicted the target genes of the 13 osteoblast-restricted mSE-miRNAs by a two-step approach. TargetScan (30) and

Table 1. Accessible long-range mSE-miRNAs and implicated hub-genes in human osteoblast mSE: GWAS SNP-mapped superenhancer. mSE-miRNA: mSE-interacted miRNA. Interaction density was the number of Hi-C interactions per Kb in mSE. Accessibility of miRNA was evaluated by open chromatin regions. There were a total of 54 unique hub-genes detected from protein–protein interaction (PPI) network, one hub-gene could be targeted by multiple miRNAs. The hub-gene marked by asterisk meant the gene has been reported by previous studies, the detailed information of relative studies was listed in Supplementary Material, Table S11. Note that for a SE mapped by multiple GWAS sets, only the best *P*-value was showed

GWAS Locus	SNP-mapped SE	Distant miRNA	*P*-value of mSE	Interactions density	Implicated hub-gene	GWAS Set
JAG1, SLX4IP	chr20: 10536348, 10656253	mir-6870	2.46E-244	0.03	DCAF7, ZFP36, AGO1, PIK3R2, DDX6, RBFOX2, ATXN1L, PAK2	Heel eBMD, LS BMD, TB BMD
SMG6	chr17: 1962802, 2042483	mir-212	6.73E-219	0.01	DYRK2*, YWHAG, MEF2A*, FOXO3*, AGO1, SOS1, PIK3R1, LYN*, PIK3CA*, FRS2, EIF4A2, UHMK1*, SMAD2*, ACVR2B*, SMAD5*, DAZAP2, ATXN1, DCUN1D1	Heel eBMD, FN BMD, TB BMD
SMG6, LOC101927839	chr17: 2115397, 2168091	mir-212	1.77E-70	0.09	–	Heel eBMD
EMP1	chr12: 13324312, 13377792	mir-614	1.67E-75	0.28	DCAF7, YWHAG	Heel eBMD
HEBP1, LOC100506314	chr12: 13128286, 13146200	mir-614	2.33E-36	0.56	–	Heel eBMD
SMG6, LOC101927839	chr17: 2115397, 2168091	mir-132	1.77E-70	0.02	DYRK2*, YWHAG, MEF2A*, FOXO3*, AGO1, SOS1, PIK3R1, LYN*, PIK3CA*, FRS2, EIF4A2, UHMK1*, SMAD2*, ACVR2B*, SMAD5*, DAZAP2, ATXN1, DCUN1D1	Heel eBMD
Intergenic	chr5: 95530421, 95595730	mir-583	1.66E-17	0.02	DYRK2*, PIK3R1, PIK3R2, EIF4A2, ZFYVE16, ACVR2B*, YWHAE, NCK2	Heel eBMD
SERTAD2	chr2: 64864825, 64889632	mir-4434	1.19E-13	0.04	FOXO3*, CBL*, PIK3R1, LYN*, PIK3CB, PRKAR1A*, CCNC, DDX6, RUNX2*, RBFOX2, ATXN1L, YWHAE, PTPN14, PAK2, SPRY2*, NECAP1	Heel eBMD
Intergenic	chr11: 121903479, 121921160	mir-125b-1	1.95E-11	0.11	YWHAG, MYCN, AGO2, FGFR2*, CCNC, TGFBR1*, SMURF1*, BMPR2*, DAZAP2, ATXN1, PRKAA2	Heel eBMD
KDM2A, ANKRD13D, ADRBK1	chr11: 67006556, 67060753	mir-6860	6.17E-08	0.02	RUNX2*, SMAD6*, SMURF1*, YAP1*, PTPN14	Heel eBMD
BCAR3	chr1: 94018520, 94142585	mir-760	2.45E-06	0.02	CBL*, NECAP1	Heel eBMD
LACTB, TPM1, RPS27L	chr15: 63305237, 63446803	mir-190a	4.06E-06	0.03	YWHAG, ZFP36, GSK3B*, MYCN, MEF2A*, ERBIN, AGO3, GAB1*, PIK3R1, PIK3CA*, PIK3CB, FGFR2*, PRKAR1A*, CNOT7*, DDX6, TGFBR1*, UHMK1*, SMAD2*, RUNX2*, SMAD6*, ACVR2B*, SMAD5*, BMPR2*, YAP1*, DAZAP2, ATXN1, ATXN1L, DCUN1D1, MOB1B, NCK2, PRKAA2, WNT5A*, WASL, NECAP1	Heel eBMD
LINC01013	chr6: 132451318, 132476057	mir-548aj-1	2.37E-05	1.01	DYRK2*, YWHAG, ZFP36, GSK3B*, ERBIN, AGO2, CBL*, GAB1*, PIK3R1, PIK3CA*, FGFR2*, FRS2, PRKAR1A*, CCNC, CNOT7*, DDX6, SMAD1*, TGFBR1*, ZFYVE16, UHMK1*, SMAD2*, SMAD6*, SMURF1*, ACVR2B*, BMPR2*, ATXN1, DCUN1D1, MOB1B, PTPN14, PAK2, PRKAA2, SPRY2*, WNT5A*	Heel eBMD
OSMR, OSMR-AS1	chr5: 38825860, 38877448	mir-3650	2.81E-05	0.02	AGO3, CCNC, SMAD1*, NCK2, PRKAA2, WASL	Heel eBMD
IRS1	chr2: 227588742, 227666687	mir-5702	3.69E-05	0.30	DCAF7, PRKAR1A*, CNOT7*	Heel eBMD

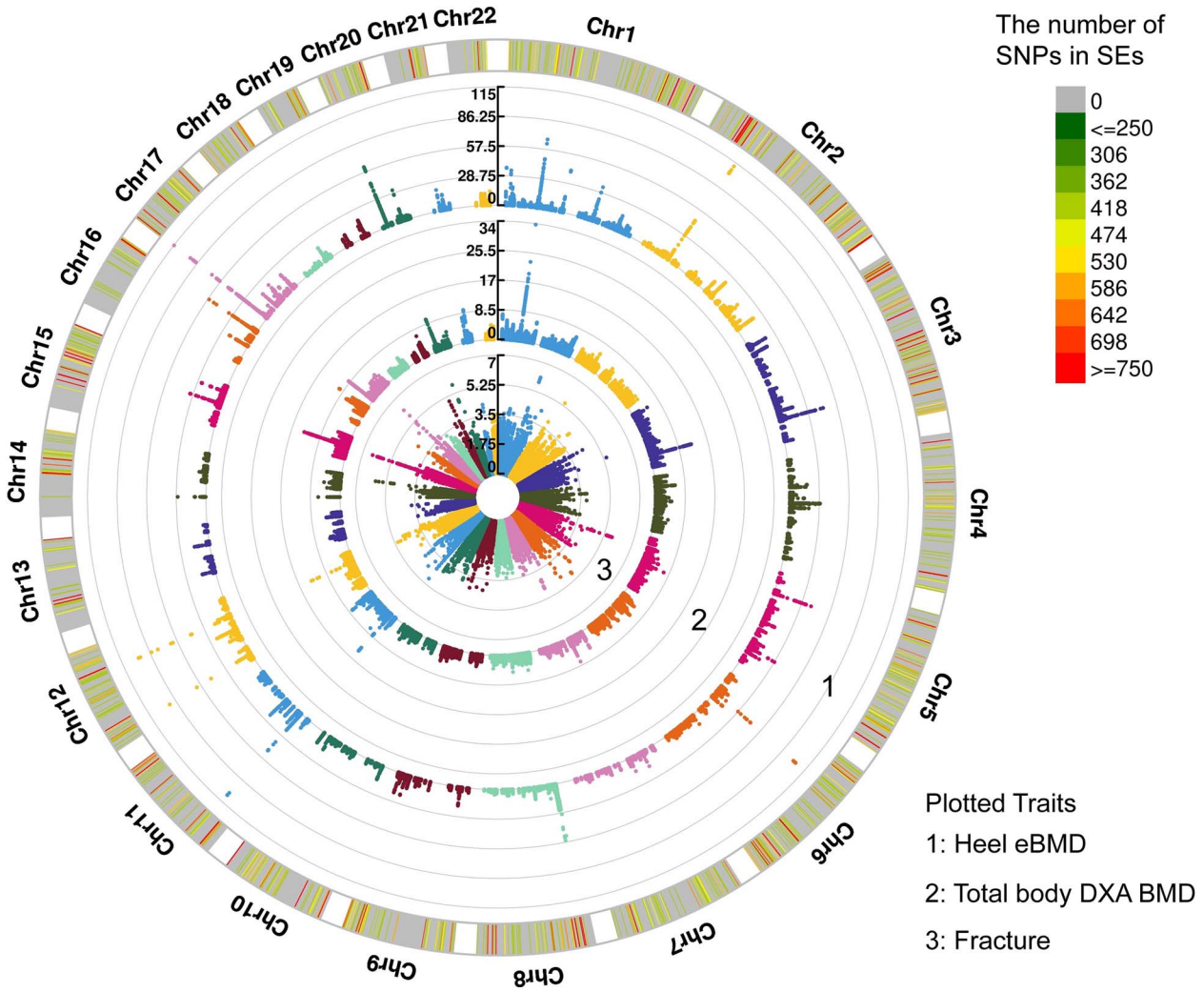

Figure 2. Genome-wide landscape of GWAS SNP loci reside in human osteoblast SEs. Each dot represented a SNP, only SE-resided SNPs were plotted, chromosomes were shown in different colors. Y-axis within each circle showed the P-value in corresponding GWAS dataset. A total of three traits, including fracture, total body DXA BMD and ultrasound estimated heel BMD (eBMD) were plotted from inside to outside. SEs loci were shown as bars within chromosomes; the color of each bar represented the number of contained SNPs. Other seven datasets included in this study were shown in Supplementary Material, Figure S3.

miRDB (31) database with their respective prediction confidence score were jointly used to form the initial pool of putative targets, and the osteoblast Ago2 CLIP-seq data was then used to filter out the false positive targets. The results showed that the number of putative targets for each miRNA was varied, miR-614 had only 21 putative targets whereas miR-548aj-3p and miR-190a-3p had 503 and 527, respectively, most of the rest of miRNAs had 100–200 putative targets (Fig. 4A). Besides, we found that the targets of miRNAs were largely shared with each other, indicating the functional similarity between them in human osteoblast (Fig. 4A). Furthermore, our results showed that miR-132-3p and miR-212-3p, which belongs to the same cluster, had almost the same putative targets. The whole lists of putative target genes of mature miRNAs were detailed in Supplementary Material, Table S8.

We performed the functional pathway and process enrichment analysis for the putative targets of each mSE-miRNA. The results of top 20 enriched Gene Ontology (GO) biological processes showed that the putative targets of miR-548aj-3p, miR-190a-3p, miR-132-3p, miR-212-3p, miR-125b-5p and miR-3650 were significantly enriched in the muscle structure development (GO Term ID: 0061061), Wnt signaling pathway (GO Term ID: 0016055), skeletal system development (GO Term ID: 0001501) and mesenchyme development (GO Term ID: 0060485), implying that these miRNAs were likely to be involved in biological processes of bone formation in human osteoblast (Fig. 4B and Supplementary Material, Table S9). Besides, we found putative targets of these miRNAs were also significantly enriched in some growth and cell differentiation pathways, such as response to growth factor (GO Term ID: 0070848) and tissue morphogenesis (GO Term ID: 0048729) (Fig. 4B), indicative of the potential effects of these miRNAs in growth and differentiation of osteoblast.

To further reveal the functional enrichment of 13 osteoblast-restricted accessible mSE-miRNAs in bone-related biological process, we extracted enrichment results of 18 GO terms (Fig. 4C) based on several key words, including ‘osteoblast’, ‘osteoclast’, ‘skeletal system’, ‘skeletal muscle’, ‘bone’, ‘ossification’, ‘BMP’ and ‘wnt signaling pathway’ from all enriched GO biological process results (Supplementary Material, Table S10). Our results showed that the skeletal system development (GO Term ID:

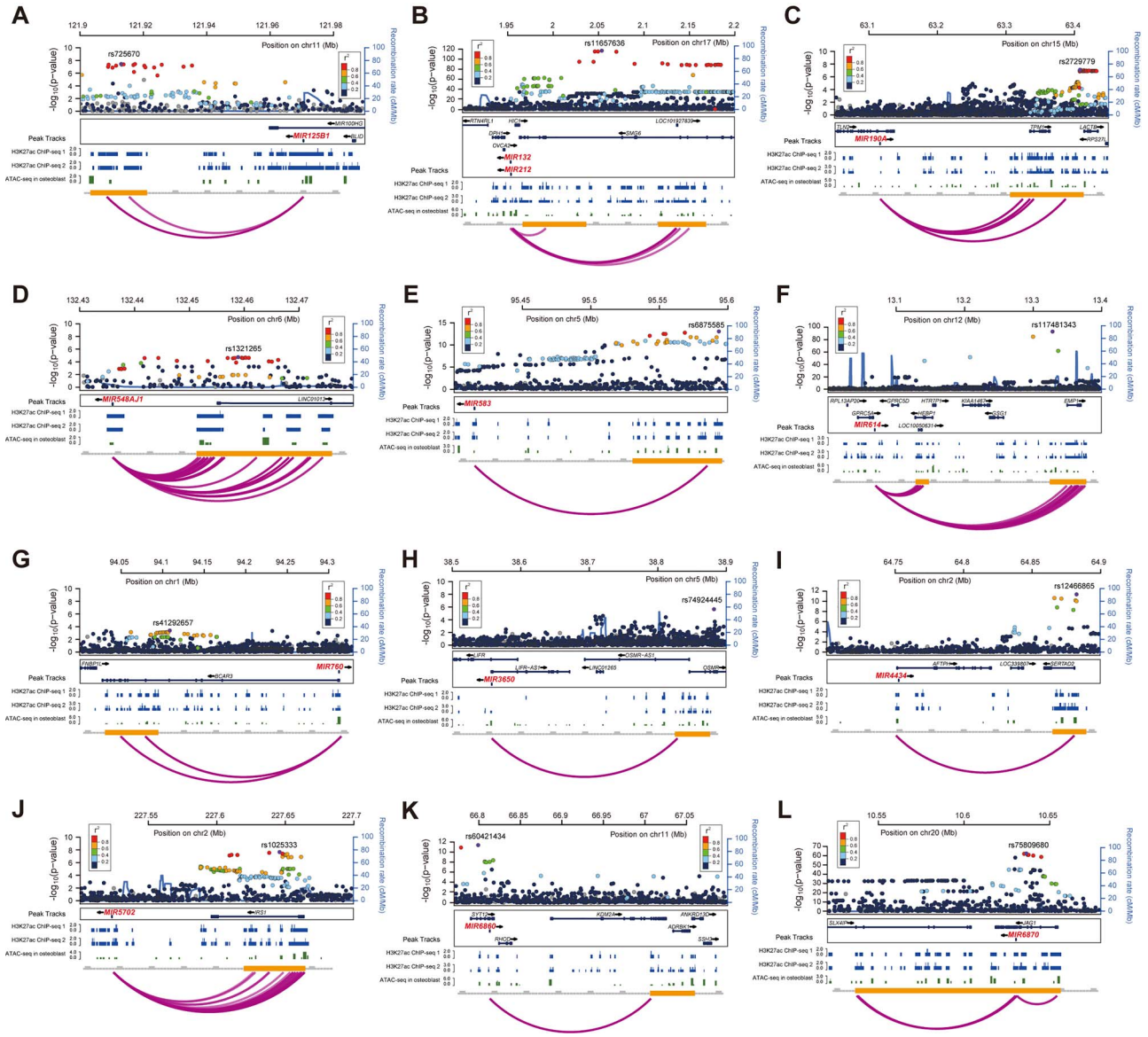

Figure 3. The regional association plots for 13 accessible mSE-miRNAs. mSE: GWAS SNP-mapped superenhancer. mSE-miRNA: mSE-interacted miRNA. The peak tracks in blue showed H3K27ac modifications in two biological replicates in osteoblast and green track showed the open chromatin regions that detected by ATAC-seq. The miRNA was considered to be accessible when the open chromatin regions found in its promoter or transcriptional start sites. The yellow bar represented SEs that were detected by ROSE and pooled in two H3K27ac datasets, and red curves represented DNA-looping interactions. Note that the genome scale for each panel was different and only most significant mapping results were plotted across all GWAS datasets. The regional associations were drawn by LocusZoom, the peak tracks and Hi-C interactions were drawn by WashU Epigenome Browser.

0001501) was enriched by the majority of the miRNAs with a high target gene ratio (Fig. 4C). Besides, the putative targets of miR-548aj-3p and miR-190a-3p were found respectively enriched in 16 and 14 out of a total of 18 bone-related processes (Fig. 4C). Two previously reported osteogenic differentiation regulator miRNAs, miR-212-3p (27) and miR-132-3p (32), were also found largely enriched in such processes (Fig. 4C). These results suggested that the osteoblast-restricted mSE-miRNAs could potentially maintain the cell identify and regulate osteogenic differentiation. However, no osteogenic process was found enriched for miR-614. Moreover, we found that the putative target genes of miR-125b-5p were largely enriched in multiple miRNA production and metabolic pathways, such as the production of miRNAs involved in gene silencing by miRNA (GO Term ID: 0035196) and the positive regulation of gene silencing by miRNA (GO Term ID: 2000637) (Fig. 4D), indicating that miR-125b-5p may act as a master miRNA to dominate the miRNA pool via SEs in osteoblast (14).

Protein–protein interaction network and hub-gene group

We next performed protein–protein interaction (PPI) network analysis for the 1279 unique putative targets of 13 osteoblast-restricted mSE-miRNAs (Supplementary Material, Table S8). A total of 54 hub-genes were finally identified as densely connected network components and constituted seven hub-gene groups [Molecular Complex Detection (MCODE1–7)] (Fig. 5A), and each hub-gene could be targeted by multiple mSE-miRNAs, indicative of a complementary regulation patterns in

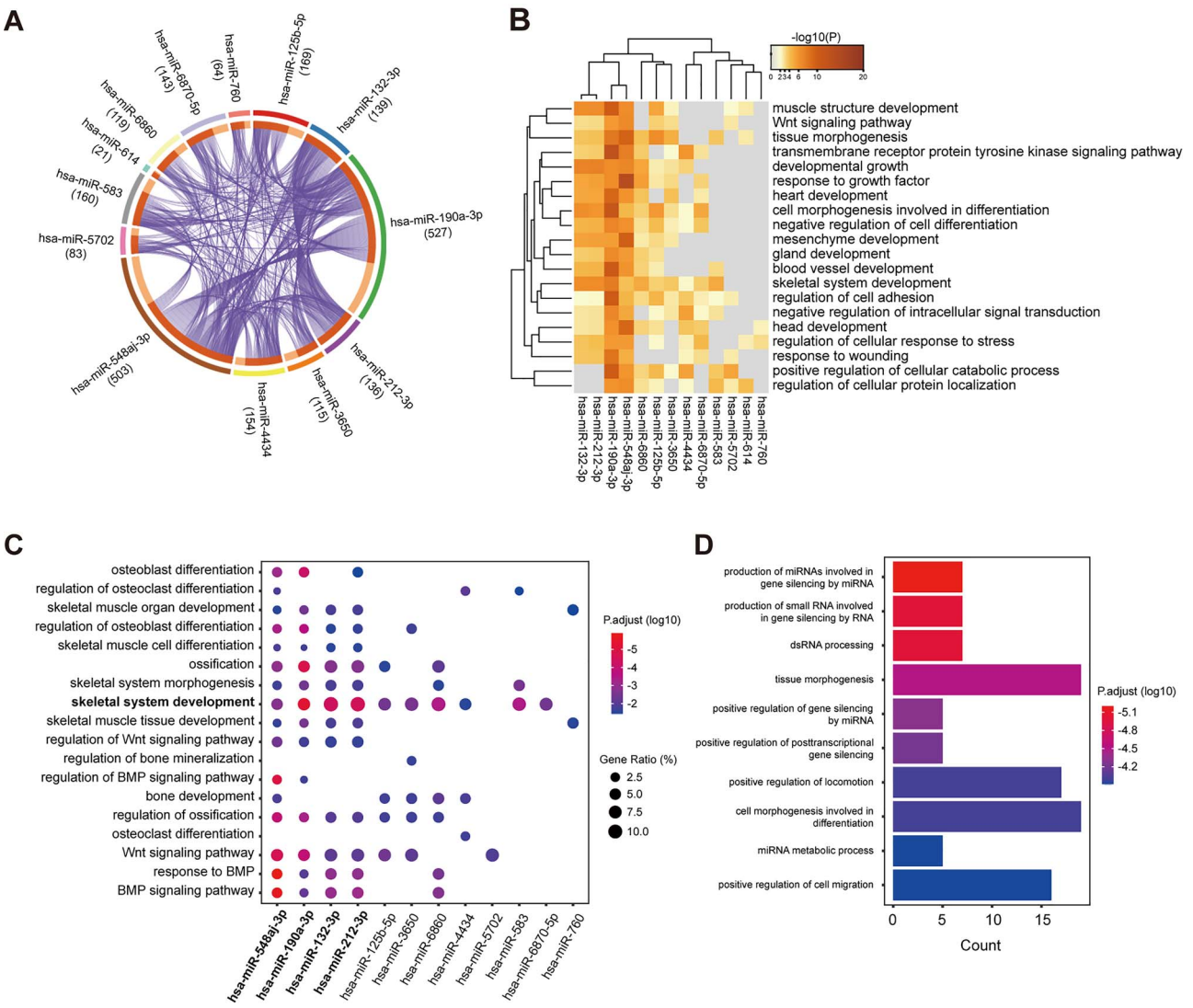

Figure 4. The top enriched biological pathways and processes for the putative targets of 13 mSE-miRNAs. (A) The numbers of putative target genes of each mSE-miRNAs, purple curves represented the targets overlapping between miRNAs. (B) The top 20 GO biological processes enrichment clusters for the putative targets of miRNAs. (C) The enrichment results in 18 osteogenic-related biological processes. Note that no such process was enriched for miR-614. (D) Top 10 enrichment results for the putative targets of miR-125b-1. All enriched GO biological process clusters for the 13 accessible mSE-miRNAs were shown in Supplementary Material, Table S10.

osteoblast (Fig. 5B). We found that there was no overlap between the genes directly resided in or near GWAS loci and the hub-genes identified in the long-range fine-mapping way by the corresponding GWAS loci (Table 1). Besides, the genes fine-mapped in this way were more than twice the corresponding GWAS loci genes (Table 1). Moreover, we investigated all 54 hub-genes identified in the long-range 'mSE-miRNA' fine-mapping approach with previous functional experiments studies, and a total of 24 of them have been found to be directly related to the bone mass and skeletal development (Supplementary Material, Table S11), whereas rest 30 have not been reported before.

We further conducted the biological pathway and process enrichment analysis for the hub-genes. Our results showed that MCODE1 group, which contained 12 hub-genes was mainly functional in mRNA cleavage involved in gene silencing processes (Table 2), suggesting an important function in the post-transcriptional regulation network; MCODE2 group genes were significantly enriched in some kinase signaling pathways, including phosphatidylinositol 3-kinase signaling (PI3K) which was implicated in osteoblast proliferation and differentiation; MCODE3 group genes were involved in cell proliferation and tissue growth of cardiac and striated muscle; besides, MCODE4 group genes we identified, including *SMAD2*, *RUNX2*, *SMAD6*, *SMURF1*, *ACVR2B*, *SMAD5*, *BMPR2* and *YAP1*, were significantly enriched in bone morphogenetic proteins (*BMP*) signaling pathway (Table 2). These results suggested that these hub-genes, which were predicted to be targeted by osteoblast-restricted mSE-miRNAs, could play a critical role in the regulation network in bone formation. The complete pathway and process enrichment results were detailed in Supplementary Material, Table S12.

Discussion

In this study, we aimed to uncover the miRNA regulatory network that was long-rang mediated by SEs which were mapped by BMD-associated SNPs in human osteoblast. We presented the landscape of BMD-related SNPs in human osteoblast SEs, and

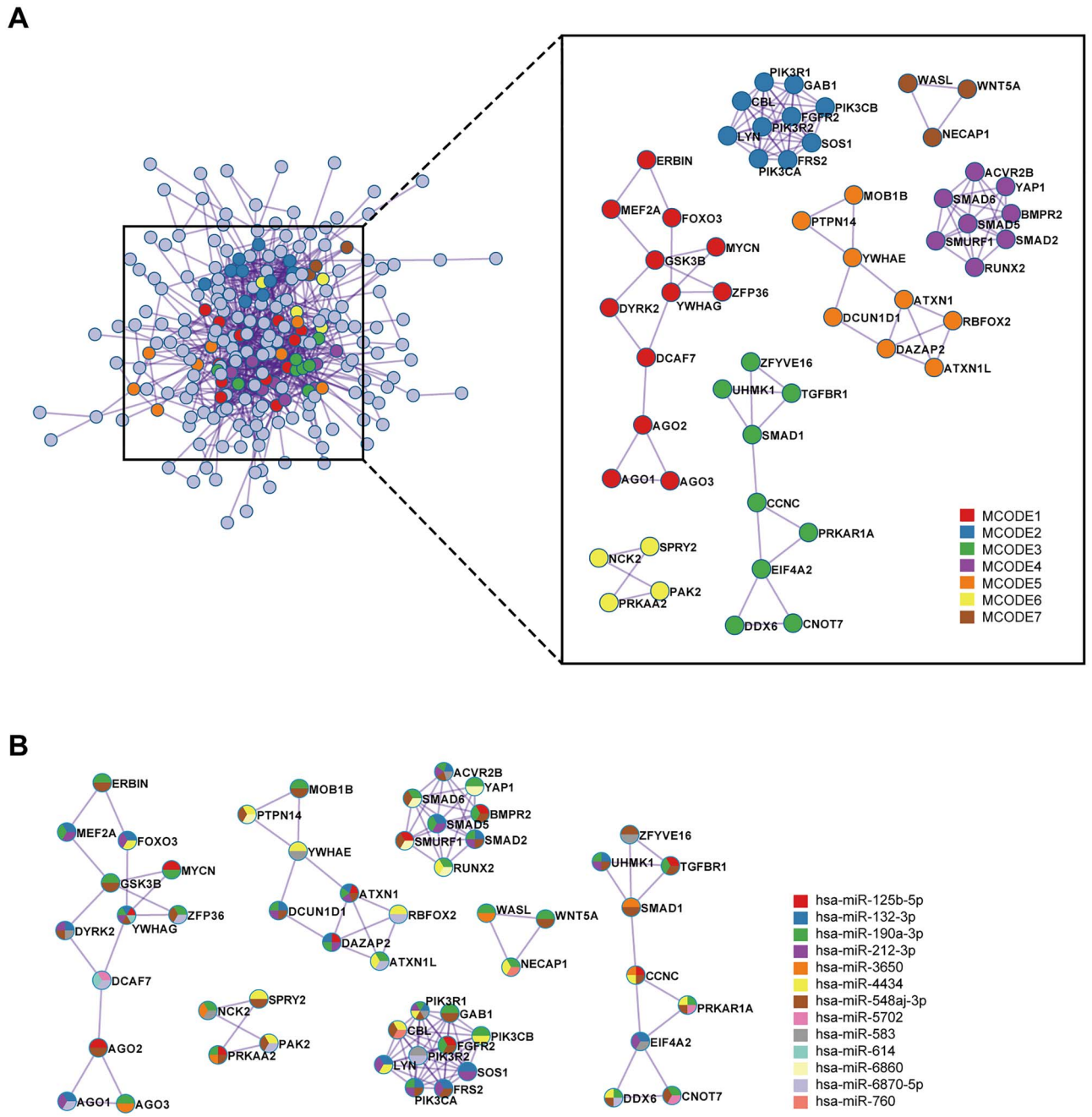

Figure 5. The protein–protein interactions network for the putative targets and 54 hub-genes in seven groups. (A) Each dot represented a putative target gene. The hub-gene groups identified by the Molecular Complex Detection algorithm were labeled by MCODE 1–7 which were zoomed in with different colors. BioGrid, InWebIM and OmniPath database were employed here for PPI network analysis. (B) All hub-genes that were predicted to be targeted by mSE-miRNAs. Each hub-gene could be targeted by multiple miRNAs.

identified 13 mSE-miRNAs and 54 genes that may maintain the osteoblast differentiation. We provided a new insight into the fine-mapping approach of GWAS loci and a tool for the genome-wide SE-based analysis and the detection of long-range osteoblast-restricted mSE-miRNAs. This approach could also be generalized to the other cell-type-specific traits or diseases.

We collected BMD-associated SNPs from large-scale human heel eBMD, DXA BMD and fracture GWAS datasets. Rather than the gene-overlapped/nearest SNPs, we focused on the long-range effective SNPs which are usually neglected in disease-associated gene selection, we assumed that a plenty of SNPs in genome are effective via affecting the SE they reside in. We plotted the SNP landscapes for 10 traits of GWAS datasets in osteoblast SEs. The genome-wide significant BMD SNP signals (P-value $< 5e{-}8$) residing in SEs were mostly from heel eBMD, followed by total body DXA BMD, while only few were from other DXA BMD, such as FN and LS (Fig. 2 and Supplementary Material, Fig. S3). Despite the BMD measurements, this disequilibrium could be mainly caused by two reasons: (i) sample size of GWAS. Heel eBMD and total body BMD GWAS was conducted in 426 824 samples and 66 628 samples, respectively. However, the samples in other datasets were <30 000, low sample size

Table 2. Seven hub-gene groups in protein–protein interaction network and the Top 3 enriched GO biological processes. For each hub-gene group, three best-enriched GO biological process terms by *P*-value were shown in the table. The enrichment was performed by MetaScape, the Banjamini–Hochberg procedure was used here for multiple testing. The complete pathway and process enrichment results for hub-gene groups were detailed in Supplementary Material, Table S12

Hub-gene group	GO terms ID	Description	P-value (log10)	MCODE Genes
MCODE1	GO:0090625	mRNA cleavage involved in gene silencing by siRNA	−9.4	DCAF7, DYRK2, YWHAG, ZFP36, GSK3B, MYCN, MEF2A, FOXO3, ERBIN, AGO1, AGO2, AGO3
	GO:0098795	mRNA cleavage involved in gene silencing	−9	
	GO:0035279	mRNA cleavage involved in gene silencing by miRNA	−9	
MCODE2	GO:0007169	Transmembrane receptor protein tyrosine kinase signaling pathway	−15.2	SOS1, CBL, GAB1, PIK3R1, PIK3R2, LYN, PIK3CA, PIK3CB, FGFR2, FRS2
	GO:0014065	Phosphatidylinositol 3-kinase (PI3K) signaling	−13.4	
	GO:0051897	Positive regulation of protein kinase B signaling	−13	
MCODE3	GO:0060038	Cardiac muscle cell proliferation	−5.8	EIF4A2, PRKAR1A, CCNC, CNOT7, DDX6, SMAD1, TGFBR1, ZFYVE16, UHMK1
	GO:0014855	Striated muscle cell proliferation	−5.5	
	GO:0055017	Cardiac muscle tissue growth	−5.2	
MCODE4	GO:0030509	BMP signaling pathway	−14.5	SMAD2, RUNX2, SMAD6, SMURF1, ACVR2B, SMAD5, BMPR2, YAP1
	GO:0071773	Cellular response to BMP stimulus	−14.2	
	GO:0071772	Response to BMP	−14.2	
MCODE5				
	GO:0051168	Nuclear export	−4.5	RBFOX2, DAZAP2, ATXN1, ATXN1L, YWHAE, DCUN1D1, MOB1B, PTPN14
	GO:0007420	Brain development	−4.3	
	GO:0060322	Head development	−4.2	
MCODE6				
	GO:0018105	Peptidyl-serine phosphorylation	−7.6	PAK2, NCK2, PRKAA2, SPRY2
	GO:0018209	Peptidyl-serine modification	−7.5	
	GO:0031400	Negative regulation of protein modification process	−6.4	
MCODE7	–	–	–	WNT5A, WASL, NECAP1

could lead to a low statistical power (33). (ii) Weight-bearing condition of different anatomical sites. The eBMD was measured at heel, which is the usually weight-bearing site of human body. Mechanical loadings and some mechanically sensitive protein, such as Piezo1, could significantly influent BMD (34); hence some SNPs for heel may be more sensitive than for other less weight-bearing anatomical sites (35).

SEs is closely related to cell-identity and fate-determined processes (15). To avoid potential biases from cell type, all data we used in this study were specific to human osteoblast, including H3K27ac ChIP-seq for SE detection, Hi-C interactions, ATAC-seq peaks for chromatin accessibility checking and CLIP-seq data for false positive target genes filtering. A total of 74 miRNAs were identified to be interacted by SNP-mapped SEs (Supplementary Material, Table S6), 12 of them have been previously found to be associated with osteogenic-related pathway, such as miR-100–5p and miR-143–3p could increase osteogenic differentiation potential by modulation of mTOR signaling (36), miR-181a could promotes osteoblastic differentiation through repression of *TGF-β* signaling molecules (37), and miR-217 in MSCs could promote cell proliferation and osteogenic differentiation by targeting *DKK1* (38) (Supplementary Material, Table S7). For the 13 accessible mSE-miRNAs, previous studies found that miR-125b (lead SNP in SE: rs725670 [G > A], BETA = 0.01 per G allele, *P*-value = 5.90E−08) could inhibit osteogenic differentiation whereas the interference of miR-212 (lead SNP in SE: rs11657636 [C > T], BETA = −0.05 per C allele, *P*-value = 4.60E-116) could promote it (26,27). In our study, the putative targets of miR-212 was largely enrich in osteogenic-related pathway and processes (Fig. 4C). In addition, we noticed that no accessible mSE-miRNA except miR-4434 was enriched in osteoclast differentiation process (Fig. 4D). This could be caused by the cell type specificity since our data were all specific to osteoblast. So far, no study reported the function of miR-4434 in bone-related tissue. Although we identified 13 mSE-miRNAs that could be potentially affected by the BMD-associated SNPs, there was a limitation in our study, we did not verify the association between such SNPs and the expression level of mSE-miRNAs. Actually, the expression quantitative trait loci (eQTL) analysis could be an approach to provide some clues. We retrieved the public eQTL databases, such as GTEx (https://www.gtexportal.org/home/), however, no bone-related tissues or osteoblastic cell-types were found.

Among the 54 hub-genes we identified, some of them were classic and well-studied osteogenic-related gene, such as *RUNX2* (Runx family transcription factor 2), *SMAD1/5* (Smad family

member 1 and 5), *BMPR2* (bone morphogenetic protein receptor type 2), *TGFBR1* (transforming growth factor beta receptor 1) and *WNT5A* (Wnt family member 5A) (39–44). In addition, the expression of some hub-genes, such as *YAP1*, *ZFP36* and *UHMK1*, were found to be up-regulated in high BMD samples (45–47). Out of a total of 54 hub-genes, 24 have been studied and found to be involved in bone formation (Supplementary Material, Table S11).

In summary, we mapped genome-wide osteoblast SEs with BMD-associated SNPs from large-scale human GWAS summary datasets. Based on that, we revealed the mSE-miRNAs regulatory network and identified 54 key genes by integrating the Hi-C, ATAC-seq and Ago2 CLIP-seq data. Our study presented the BMD-related SNP loci landscape in SEs, and provided a new approach and insight for the fine-mapping of GWAS loci. We also provided a tool for the genome-wide SE-based analysis and the detection of long-range osteoblast-restricted mSE-miRNAs (https://github.com/Zheng-Lab-Westlake/Osteo-Fine-Mapp-SNP2SE2miRNA).

Materials and Methods

GWAS summary-statistic data

The overall study design was shown in Figure 1. We included 10 GWAS summary-statistic datasets of different BMD-related traits from Genetic Factors for Osteoporosis (GEFOS) Consortium, which is a large international collaborative effort we were involved in. The fracture summary statistics data were obtained from a study with ∼2.5 million SNPs in 20 439 fracture cases and 78 843 controls (1), and from UK biobank with ∼14 million SNPs in 53 184 fracture cases and 373 611 controls (7). The eBMD GWAS dataset was from UK biobank which contained ∼13.8 million SNPs in 426 824 samples (7). The DXA BMD at distal radius/FA, FN and LS were from UK10K project which included ∼10 million SNPs in 8143 samples, 29 188 samples and 25 225 samples, respectively (5). In addition, we included FN and LS DXA BMD GWAS data from another study which included ∼2.5 million SNPs in 32 961 and 31 800 samples, respectively (3). We also included GWAS summary-statistic data of total body DXA BMD (∼18.3 million SNPs in 66 628 samples) (6) and total body less head DXA BMD (∼2.3 million SNPs in 10 414 samples) (48). All datasets which were not based on hg19 were lifted over to hg19 by liftover tool in UCSC (http://genome.ucsc.edu/). And all GWAS summary-statistic datasets used in this study were listed in Supplementary Material, Table S13.

Detection of SE in human osteoblast

SEs are usually modified by H3K27ac marks (18), hence we used the H3K27ac ChIP-seq data to detect SEs. The BAM data of H3K27ac ChIP-seq (ENCODE accession: ENCSR000APH) with two biological replications in human primary osteoblast and the control data (ENCODE accession: ENCSR000APU) were downloaded from the ENCODE Project (49). We performed quality control for the alignment datasets by SAMtools (50), PCR duplicate reads and any reads with Q-value < 20 were removed. The MACS2 was employed for peak calling with default settings (51), resulting 72 936 and 116 190 narrow peaks for two replications, respectively. Next, we employed the ROSE algorithm to identify the SE regions (17), in brief, H3K27ac peaks within 2.5 kb of TSS on genome were subtracted and the enhancers within a distance of 12.5 kb were stitched according to H3K27ac peaks occupancy rates (52). Finally, we plotted the ranked stitched enhancers and individual enhancers by H3K27ac enrichment, and using a line with a slope of one tangent to the curve as a cutoff to distinguish SEs above the point and typical enhancers below the point of tangency.

We downloaded the human osteoblast SEs from SEA and dbSUPER database (53,54), and the human fetal osteoblasts (hFOB, undifferentiated and differentiated) SEs from SEdb (55). The Wash U Epigenome Browser (http://epigenomegateway.wustl.edu/browser/) was employed (56) to compare the SEs from the databases with the SEs identified in our study by visualizing the results.

Genome-wide SE-based analysis in human osteoblast

For the SEs we detected in human osteoblast, we first mapped them with SNPs ($P < 0.05$) in 10 BMD-related GWAS datasets to investigate the landscape of SNP resided in SEs. And then we performed the SE-based mapping analysis by the independent SNPs. We extracted the EUR group genotypes (European ancestry) in 1000 Genome Project Phase 3 (1000GP, v5a) (57) as the SNPs reference and calculated the r^2 by PLINK v1.9 with setting window size at 50 SNP counts, step size at five counts (58). The non-independent SNPs with $r^2 > 0.1$ were then pruned out. We next mapped SE by the GLOSSI methods (59), the statistic for each SE was defined as below:

$$S_k = -2\sum_{j=1}^{J} g_{jk} \ln(p_j) \quad (1)$$

Where g_{jk} is an indicator variable for each SE_k and each SNP_j, $g_{jk} = 1$ if SNP_j is in SE_k, $g_{jk} = 0$ otherwise; p_j is the P-value of SNP_j in GWAS summary data. Based on Fisher's transformation, we calculated the P-value for SE_k using corresponding χ^2 distribution. The Bonferroni correction was then employed for the multitest, SNP-mapped SE (mSE) with P-value <4.08e−5 (0.05/1224 for biological replicate 1) or 4.35e−5 (0.05/1149 for biological replicate 2) were regarded to be significant.

Identification of long-range interactions between pri-miRNA and SEs in human osteoblast

The human miRNA data were downloaded from miRBase v22 (60), a total of 1914 pri-miRNAs transcripts and 2880 mature miRNAs were included. Note that the genome positions of miRNAs were lifted over from GRCh38 to hg19 since the miRBase v22 only provided miRNA in GRCh38 version. For each pri-miRNA, we designed its promoter baits region. Since only a part of TSS of pri-miRNAs were available, we employed two strategies for that here: (i) using the miRNA gene promoter baits which were designed by SureSelect library (Agilent) targeted TSSs in Alessandra Chesi *et al.* study (9); (ii) we obtained the TSS of pri-miRNAs from miRGen v3 database (61), and defined the promoter region of a particular pri-miRNA as the 2.5 kb upstream region before the TSS or itself. Finally, there were 1549 promoter baits region were obtained from Agilent SureSelect library, and 365 putative promoter baits regions were designed using miRGen v3 TSS or the pri-miRNAs-self (Supplementary Material, Table S5).

We obtained the high-resolution genome-scale, promoter-focused Capture C data and ATAC-seq data in primary MSCs-derived osteoblasts from ArrayExpress (E-MTAB-6862, E-MTAB-6834) (9), including 295 422 DNA-looping interactions (1-fragment and 4-fragment resolutions) and 156 406 ATAC-seq peaks. Note that these data we downloaded were not raw but had been processed using CHiCAGO and ENCODE ATAC-seq pipeline (https://github.com/kundajelab/atac_dnase_pipelines),

the processing steps, including quality control, were detailed in the original study (9). Then, we overlapped the genome-wide long-range interactions regions with the promoter of pri-miRNAs and significant mSEs we detected, respectively. For the long-range mSEs-interacted miRNAs (mSE-miRNAs), we further investigated the chromatin accessibility by overlapping them with ATAC-seq peaks. The mSE-miRNAs with open chromatin region in the promoter or TSS was considered to be accessible. The LocusZoom and WashU Epigenome Browser were employed for results plotting (62,63). Here, we developed a tool for the genome-wide SE-based analysis and the detection of long-range osteoblast-restricted mSE-miRNAs (https://github.com/Zheng-Lab-Westlake/Osteo-Fine-Mapp-SNP2SE2miRNA).

Target gene prediction of accessible mSE-miRNAs

We used a two-steps approach to predicted target genes of accessible mSE-miRNAs. First step, we accessed TargetScan v7.2 and miRDB v6.0 (30,31), the two most commonly used miRNA targets database, to initially conduct the prediction. For TargetScan results, any targets predicted with the absolute value of cumulative weighted context++ scores (CWCS) <0.2 will be filtered out, CWCS was a specific value that provided by TargetScan algorithm for the measurement of prediction confidence (30). For miRDB results, a prediction score ranged from 50 to 100 was used to measure the confidence (31). And as the database developer recommended, any target with the score <60 will be excluded. The union of results of both databases was then formed as the initial target genes pool. Second step, we downloaded the osteoblasts-specific Ago2 CLIP-seq data from GEO (GSE111432) (64), and downloaded the 3′ UTR RefSeq (hg19) of human genes from UCSC (http://genome.ucsc.edu/). We called the peaks from the bedGraph data of Ago2 CLIP-seq by using MACS2 bdgpeakcall utility (51). The 3′ UTR of predicted target genes were then overlapped with the Ago2 CLIP-seq peaks. Any targets failed the overlapping will be considered as false positive target and filtered out from prediction pool. Beside, for the pairwise mature miRNAs (i.e. -5p/−3p) that were derived from the same pri-miRNA, we found that the quantity of final targets was greatly different from each other, including miR-125b-5p/−1-3p (169 versus 37), miR-190a-5p/−3p (69 versus 527), miR-132-5p/−3p (45 versus 139), miR-212-5p/−3p (66 versus 136) and miR-6870-5p/−3p (143 versus 44) (Supplementary Material, Table S8). Here, only the one with more targets in each mature miRNA pair was kept for next analysis because of the quantity difference and overlapping of targets.

Biological pathway and process enrichment analysis

For the putative target genes of 13 accessible mSE-miRNAs, we performed biological pathway and process enrichment analysis using the web-based tool metaScape (65) and R package clusterProfiler (66). Enriched terms with a P-value < 0.01, a minimum miRNA target genes count of 3, and a ratio between the observed counts and the counts expected by chance >1.5 (enrichment factor) were collected and grouped into clusters based on their membership similarities (65). The Banjamini–Hochberg procedure was used here for multiple testing (67). For enriched pathway and process clusters across the 13 miRNAs, hierarchical clustering was then performed by metaScape pipeline.

Hub-gene detection and enrichment analysis

We next performed PPI network analysis with the following database BioGrid (68), InWebIM and OmniPath (69) on the metaScape platform. The PPI network contains the subset of proteins that form physical interactions with at least one other member in the putative target genes of 13 mSE-miRNAs. MCODE algorithm (70) was then applied to identify hub-gene groups from the PPI network with default settings. Next, for each hub-gene group identified, the GO biological process enrichment analysis was applied independently using metaScape pipeline (65), and the three best-enriched terms by P-value were used as the functional description of the corresponding components.

Supplementary Material

Supplementary Material is available at *HMG* online.

Acknowledgements

We thankfully acknowledge Nan Li from the High-Performance Computing Center at Westlake University for the facility support and technical assistance. We thank the GEFOS Consortium to provide the GWAS summary data. We thank all the public databases and studies who supported this work, especially for the Alessandra Chesi's study. We also thank the peer reviewers for their thorough and helpful review of this manuscript.

Conflict of Interest statement. None declared.

Funding

National Natural Science Foundation of China (Grants No: 81871831 and 32061143019).

References

1. Trajanoska, K., Morris, J.A., Oei, L., Zheng, H.F., Evans, D.M., Kiel, D.P., Ohlsson, C., Richards, J.B., Rivadeneira, F., Consortium, G.G. *et al.* (2018) Assessment of the genetic and clinical determinants of fracture risk: genome wide association and mendelian randomisation study. *BMJ*, **362**, k3225.
2. Cauley, J.A., Hochberg, M.C., Lui, L.Y., Palermo, L., Ensrud, K.E., Hillier, T.A., Nevitt, M.C. and Cummings, S.R. (2007) Long-term risk of incident vertebral fractures. *JAMA*, **298**(23), 2761–2767.
3. Estrada, K., Styrkarsdottir, U., Evangelou, E., Hsu, Y.H., Duncan, E.L., Ntzani, E.E., Oei, L., Albagha, O.M., Amin, N., Kemp, J.P. *et al.* (2012) Genome-wide meta-analysis identifies 56 bone mineral density loci and reveals 14 loci associated with risk of fracture. *Nat. Genet.*, **44**(5), 491–501.
4. Rivadeneira, F., Styrkarsdottir, U., Estrada, K., Halldorsson, B.V., Hsu, Y.H., Richards, J.B., Zillikens, M.C., Kavvoura, F.K., Amin, N., Aulchenko, Y.S. *et al.* (2009) Twenty bone-mineral-density loci identified by large-scale meta-analysis of genome-wide association studies. *Nat. Genet.*, **41**, 1199–1206.
5. Zheng, H.F., Forgetta, V., Hsu, Y.H., Estrada, K., Rosello-Diez, A., Leo, P.J., Dahia, C.L., Park-Min, K.H., Tobias, J.H., Kooperberg, C. *et al.* (2015) Whole-genome sequencing identifies EN1 as a determinant of bone density and fracture. *Nature*, **526**(7571), 112–117.
6. Medina-Gomez, C., Kemp, J.P., Trajanoska, K., Luan, J., Chesi, A., Ahluwalia, T.S., Mook-Kanamori, D.O., Ham, A., Hartwig, F.P., Evans, D.S. *et al.* (2018) Life-course genome-wide association study meta-analysis of total body BMD and assessment of age-specific effects. *Am. J. Hum. Genet.*, **102**(1), 88–102.
7. Morris, J.A., Kemp, J.P., Youlten, S.E., Laurent, L., Logan, J.G., Chai, R.C., Vulpescu, N.A., Forgetta, V., Kleinman, A.,

Mohanty, S.T. *et al.* (2019) An atlas of genetic influences on osteoporosis in humans and mice. *Nat. Genet.*, **51**(2), 258–266.
8. Spain, S.L. and Barrett, J.C. (2015) Strategies for fine-mapping complex traits. *Hum. Mol. Genet.*, **24**(R1), R111–R119.
9. Chesi, A., Wagley, Y., Johnson, M.E., Manduchi, E., Su, C., Lu, S., Leonard, M.E., Hodge, K.M., Pippin, J.A., Hankenson, K.D. *et al.* (2019) Genome-scale capture C promoter interactions implicate effector genes at GWAS loci for bone mineral density. *Nat. Commun.*, **10**(1), 1260.
10. Smemo, S., Tena, J.J., Kim, K.H., Gamazon, E.R., Sakabe, N.J., Gomez-Marin, C., Aneas, I., Credidio, F.L., Sobreira, D.R., Wasserman, N.F. *et al.* (2014) Obesity-associated variants within FTO form long-range functional connections with IRX3. *Nature*, **507**(7492), 371–375.
11. Mifsud, B., Tavares-Cadete, F., Young, A.N., Sugar, R., Schoenfelder, S., Ferreira, L., Wingett, S.W., Andrews, S., Grey, W., Ewels, P.A. *et al.* (2015) Mapping long-range promoter contacts in human cells with high-resolution capture hi-C. *Nat. Genet.*, **47**(6), 598–606.
12. Eagen, K.P. (2018) Principles of chromosome architecture revealed by hi-C. *Trends Biochem. Sci.*, **43**, 469–478.
13. Whyte, W.A., Orlando, D.A., Hnisz, D., Abraham, B.J., Lin, C.Y., Kagey, M.H., Rahl, P.B., Lee, T.I. and Young, R.A. (2013) Master transcription factors and mediator establish super-enhancers at key cell identity genes. *Cell*, **153**(2), 307–319.
14. Suzuki, H.I., Young, R.A. and Sharp, P.A. (2017) Super-enhancer-mediated RNA processing revealed by integrative MicroRNA network analysis. *Cell*, **168**(6), 1000, e1015–1014.
15. Hnisz, D., Abraham, B.J., Lee, T.I., Lau, A., Saint-Andre, V., Sigova, A.A., Hoke, H.A. and Young, R.A. (2013) Super-enhancers in the control of cell identity and disease. *Cell*, **155**(4), 934–947.
16. Zamudio, A.V., Dall'Agnese, A., Henninger, J.E., Manteiga, J.C., Afeyan, L.K., Hannett, N.M., Coffey, E.L., Li, C.H., Oksuz, O., Sabari, B.R. *et al.* (2019) Mediator condensates localize signaling factors to key cell identity genes. *Mol. Cell*, **76**(5), 753, e756–766.
17. Loven, J., Hoke, H.A., Lin, C.Y., Lau, A., Orlando, D.A., Vakoc, C.R., Bradner, J.E., Lee, T.I. and Young, R.A. (2013) Selective inhibition of tumor oncogenes by disruption of super-enhancers. *Cell*, **153**(2), 320–334.
18. Pott, S. and Lieb, J.D. (2015) What are super-enhancers? *Nat. Genet.*, **47**(1), 8–12.
19. Ernst, J., Kheradpour, P., Mikkelsen, T.S., Shoresh, N., Ward, L.D., Epstein, C.B., Zhang, X., Wang, L., Issner, R., Coyne, M. *et al.* (2011) Mapping and analysis of chromatin state dynamics in nine human cell types. *Nature*, **473**(7345), 43–49.
20. Pasquali, L., Gaulton, K.J., Rodriguez-Segui, S.A., Mularoni, L., Miguel-Escalada, I., Akerman, I., Tena, J.J., Moran, I., Gomez-Marin, C., van de Bunt, M. *et al.* (2014) Pancreatic islet enhancer clusters enriched in type 2 diabetes risk-associated variants. *Nat. Genet.*, **46**(2), 136–143.
21. Lian, J.B., Stein, G.S., van Wijnen, A.J., Stein, J.L., Hassan, M.Q., Gaur, T. and Zhang, Y. (2012) MicroRNA control of bone formation and homeostasis. *Nat. Rev. Endocrinol.*, **8**(4), 212–227.
22. Moore, B.T. and Xiao, P. (2013) MiRNAs in bone diseases. *Microrna*, **2**(1), 20–31.
23. Wu, T., Zhou, H., Hong, Y., Li, J., Jiang, X. and Huang, H. (2012) miR-30 family members negatively regulate osteoblast differentiation. *J. Biol. Chem.*, **287**(10), 7503–7511.
24. Wang, T. and Xu, Z. (2010) miR-27 promotes osteoblast differentiation by modulating Wnt signaling. *Biochem. Biophys. Res. Commun.*, **402**(2), 186–189.
25. Bae, Y., Yang, T., Zeng, H.C., Campeau, P.M., Chen, Y., Bertin, T., Dawson, B.C., Munivez, E., Tao, J. and Lee, B.H. (2012) miRNA-34c regulates Notch signaling during bone development. *Hum. Mol. Genet.*, **21**(13), 2991–3000.
26. Mizuno, Y., Yagi, K., Tokuzawa, Y., Kanesaki-Yatsuka, Y., Suda, T., Katagiri, T., Fukuda, T., Maruyama, M., Okuda, A., Amemiya, T. *et al.* (2008) miR-125b inhibits osteoblastic differentiation by down-regulation of cell proliferation. *Biochem. Biophys. Res. Commun.*, **368**(2), 267–272.
27. Zhang, Y., Jiang, Y., Luo, Y. and Zeng, Y. (2020) Interference of miR-212 and miR-384 promotes osteogenic differentiation via targeting RUNX2 in osteoporosis. *Exp. Mol. Pathol.*, **113**, 104366. 10.1016/j.yexmp.2019.104366.
28. Kapinas, K. and Delany, A.M. (2011) MicroRNA biogenesis and regulation of bone remodeling. *Arthritis Res Ther*, **13**(3), 220. 10.1186/ar3325.
29. Park, C.Y., Choi, Y.S. and McManus, M.T. (2010) Analysis of microRNA knockouts in mice. *Hum. Mol. Genet.*, **19**(R2), R169–R175.
30. Agarwal, V., Bell, G.W., Nam, J.W. and Bartel, D.P. (2015) Predicting effective microRNA target sites in mammalian mRNAs. *Elife*, **4**, e05005. 10.7554/eLife.05005.
31. Chen, Y. and Wang, X. (2020) miRDB: an online database for prediction of functional microRNA targets. *Nucleic Acids Res.*, **48**(D1, D1), D127–D131.
32. Qu, X., Chen, Z., Fan, D., Sun, C. and Zeng, Y. (2016) MiR-132-3p regulates the osteogenic differentiation of thoracic ligamentum Flavum cells by inhibiting multiple osteogenesis-related genes. *Int. J. Mol. Sci.*, **17**(8), 1370. 10.3390/ijms17081370.
33. Dumas-Mallet, E., Button, K.S., Boraud, T., Gonon, F. and Munafo, M.R. (2017) Low statistical power in biomedical science: a review of three human research domains. *R. Soc. Open Sci.*, **4**(2), 160254. 10.1098/rsos.160254.
34. Wang, L., You, X., Lotinun, S., Zhang, L., Wu, N. and Zou, W. (2020) Mechanical sensing protein PIEZO1 regulates bone homeostasis via osteoblast-osteoclast crosstalk. *Nat. Commun.*, **11**(1), 282. 10.1038/s41467-019-14146-6.
35. Bai, W.Y., Wang, L., Ying, Z.M., Hu, B., Xu, L., Zhang, G.Q., Cong, P.K., Zhu, X., Zou, W. and Zheng, H.F. (2020) Identification of PIEZO1 polymorphisms for human bone mineral density. *Bone*, **133**, 115247. 10.1016/j.bone.2020.115247.
36. Frith, J.E., Kusuma, G.D., Carthew, J., Li, F., Cloonan, N., Gomez, G.A. and Cooper-White, J.J. (2018) Mechanically-sensitive miRNAs bias human mesenchymal stem cell fate via mTOR signalling. *Nat. Commun.*, **9**(1), 257. 10.1038/s41467-017-02486-0.
37. Bhushan, R., Grunhagen, J., Becker, J., Robinson, P.N., Ott, C.E. and Knaus, P. (2013) miR-181a promotes osteoblastic differentiation through repression of TGF-beta signaling molecules. *Int. J. Biochem. Cell Biol.*, **45**(3), 696–705.
38. Dai, Z., Jin, Y., Zheng, J., Liu, K., Zhao, J., Zhang, S., Wu, F. and Sun, Z. (2019) MiR-217 promotes cell proliferation and osteogenic differentiation of BMSCs by targeting DKK1 in steroid-associated osteonecrosis. *Biomed. Pharmacother.*, **109**, 1112–1119.
39. Wei, J., Shimazu, J., Makinistoglu, M.P., Maurizi, A., Kajimura, D., Zong, H., Takarada, T., Lezaki, T., Pessin, J.E., Hinoi, E. *et al.* (2015) Glucose uptake and Runx2 synergize to orchestrate osteoblast differentiation and bone formation. *Cell*, **161**(7), 1576–1591.
40. Miyazono, K. (2000) TGF-beta signaling by Smad proteins. *Cytokine Growth Factor Rev.*, **11**(1–2), 15–22.

41. Hogan, B.L. (1996) Bone morphogenetic proteins: multifunctional regulators of vertebrate development. *Genes Dev.*, **10**(13), 1580–1594.
42. Roberts, J.L., Liu, G., Paglia, D.N., Kinter, C.W., Fernandes, L.M., Lorenzo, J., Hansen, M.F., Arif, A. and Drissi, H. (2020) Deletion of Wnt5a in osteoclasts results in bone loss through decreased bone formation. *Ann. N. Y. Acad. Sci.*, **1463**(1), 45–59.
43. Quinn, J.M., Itoh, K., Udagawa, N., Hausler, K., Yasuda, H., Shima, N., Mizuno, A., Higashio, K., Takahashi, N., Suda, T. *et al.* (2001) Transforming growth factor beta affects osteoclast differentiation via direct and indirect actions. *J. Bone Miner. Res.*, **16**(10, 10), 1787–1794.
44. Hu, H., Hilton, M.J., Tu, X., Yu, K., Ornitz, D.M. and Long, F. (2005) Sequential roles of Hedgehog and Wnt signaling in osteoblast development. *Development*, **132**(1, 1), 49–60.
45. Huang, Y., Xiao, D., Huang, S., Zhuang, J., Zheng, X., Chang, Y. and Yin, D. (2020) Circular RNA YAP1 attenuates osteoporosis through up-regulation of YAP1 and activation of Wnt/beta-catenin pathway. *Biomed. Pharmacother.*, **129**, 110365. 10.1016/j.biopha.2020.110365.
46. Zhang, H., Feng, J., Lin, Z., Wang, S., Wang, Y., Dai, S., Kong, W., Wang, Y. and Zhang, Z. (2020) Identification and analysis of genes underlying bone mineral density by integrating microarray data of osteoporosis. *Front Cell Dev Biol*, **8**, 798. 10.3389/fcell.2020.00798.
47. Choi, H.J., Park, H., Zhang, L., Kim, J.H., Kim, Y.A., Yang, J.Y., Pei, Y.F., Tian, Q., Shen, H., Hwang, J.Y. *et al.* (2016) Genome-wide association study in East Asians suggests UHMK1 as a novel bone mineral density susceptibility gene. *Bone*, **91**, 113–121.
48. Medina-Gomez, C., Kemp, J.P., Dimou, N.L., Kreiner, E., Chesi, A., Zemel, B.S., Bonnelykke, K., Boer, C.G., Ahluwalia, T.S., Bisgaard, H. *et al.* (2017) Bivariate genome-wide association meta-analysis of pediatric musculoskeletal traits reveals pleiotropic effects at the SREBF1/TOM1L2 locus. *Nat. Commun.*, **8**, 121.
49. Consortium, E.P (2012) An integrated encyclopedia of DNA elements in the human genome. *Nature*, **489**(7414), 57–74.
50. Li, H., Handsaker, B., Wysoker, A., Fennell, T., Ruan, J., Homer, N., Marth, G., Abecasis, G., Durbin, R. and Genome Project Data Processing, S (2009) The sequence alignment/map format and SAMtools. *Bioinformatics*, **25**(16), 2078–2079.
51. Feng, J., Liu, T., Qin, B., Zhang, Y. and Liu, X.S. (2012) Identifying ChIP-seq enrichment using MACS. *Nat. Protoc.*, **7**(9), 1728–1740.
52. Jia, Y., Chng, W.J. and Zhou, J. (2019) Super-enhancers: critical roles and therapeutic targets in hematologic malignancies. *J. Hematol. Oncol.*, **12**, 77.
53. Chen, C., Zhou, D., Gu, Y., Wang, C., Zhang, M., Lin, X., Xing, J., Wang, H. and Zhang, Y. (2020) SEA version 3.0: a comprehensive extension and update of the super-enhancer archive. *Nucleic Acids Res.*, **48**, D198–D203.
54. Khan, A. and Zhang, X. (2016) dbSUPER: a database of super-enhancers in mouse and human genome. *Nucleic Acids Res.*, **44**, D164–D171.
55. Jiang, Y., Qian, F., Bai, X., Liu, Y., Wang, Q., Ai, B., Han, X., Shi, S., Zhang, J., Li, X. *et al.* (2019) SEdb: a comprehensive human super-enhancer database. *Nucleic Acids Res.*, **47**, D235–D243.
56. Zhou, X. and Wang, T. (2012) Using the Wash U Epigenome Browser to examine genome-wide sequencing data. *Curr. Protoc. Bioinform.*, **40**, 10.10.1–10.10.14.
57. Genomes Project, C., Auton, A., Brooks, L.D., Durbin, R.M., Garrison, E.P., Kang, H.M., Korbel, J.O., Marchini, J.L., McCarthy, S., McVean, G.A. *et al.* (2015) A global reference for human genetic variation. *Nature*, **526**, 68–74.
58. Chang, C.C., Chow, C.C., Tellier, L.C., Vattikuti, S., Purcell, S.M. and Lee, J.J. (2015) Second-generation PLINK: rising to the challenge of larger and richer datasets. *Gigascience*, **4**, 7.
59. Chai, H.S., Sicotte, H., Bailey, K.R., Turner, S.T., Asmann, Y.W. and Kocher, J.P. (2009) GLOSSI: a method to assess the association of genetic loci-sets with complex diseases. *BMC Bioinform.*, **10**, 102.
60. Kozomara, A., Birgaoanu, M. and Griffiths-Jones, S. (2019) miRBase: from microRNA sequences to function. *Nucleic Acids Res.*, **47**, D155–D162.
61. Georgakilas, G., Vlachos, I.S., Zagganas, K., Vergoulis, T., Paraskevopoulou, M.D., Kanellos, I., Tsanakas, P., Dellis, D., Fevgas, A., Dalamagas, T. *et al.* (2016) DIANA-miRGen v3.0: accurate characterization of microRNA promoters and their regulators. *Nucleic Acids Res.*, **44**, D190–D195.
62. Pruim, R.J., Welch, R.P., Sanna, S., Teslovich, T.M., Chines, P.S., Gliedt, T.P., Boehnke, M., Abecasis, G.R. and Willer, C.J. (2010) LocusZoom: regional visualization of genome-wide association scan results. *Bioinformatics*, **26**, 2336–2337.
63. Zhou, X., Li, D., Zhang, B., Lowdon, R.F., Rockweiler, N.B., Sears, R.L., Madden, P.A., Smirnov, I., Costello, J.F. and Wang, T. (2015) Epigenomic annotation of genetic variants using the Roadmap Epigenome Browser. *Nat. Biotechnol.*, **33**, 345–346.
64. Jung, E., Seong, Y., Jeon, B., Kwon, Y.S. and Song, H. (2018) MicroRNAs of miR-17-92 cluster increase gene expression by targeting mRNA-destabilization pathways. *Biochim. Biophys. Acta Gene. Regul. Mech.*, **1861**, 603–612.
65. Zhou, Y., Zhou, B., Pache, L., Chang, M., Khodabakhshi, A.H., Tanaseichuk, O., Benner, C. and Chanda, S.K. (2019) Metascape provides a biologist-oriented resource for the analysis of systems-level datasets. *Nat. Commun.*, **10**, 1523.
66. Yu, G., Wang, L.G., Han, Y. and He, Q.Y. (2012) clusterProfiler: an R package for comparing biological themes among gene clusters. *OMICS*, **16**, 284–287.
67. Hochberg, Y. and Benjamini, Y. (1990) More powerful procedures for multiple significance testing. *Stat. Med.*, **9**, 811–818.
68. Breitkreutz, B.J., Stark, C. and Tyers, M. (2002) The GRID: the general repository for interaction datasets. *Genome Biol.*, **4**, R23. 10.1186/gb-2003-4-3-r23.
69. Li, T., Wernersson, R., Hansen, R.B., Horn, H., Mercer, J., Slodkowicz, G., Workman, C.T., Rigina, O., Rapacki, K., Staerfeldt, H.H. *et al.* (2017) A scored human protein-protein interaction network to catalyze genomic interpretation. *Nat. Methods*, **14**, 61–64.
70. Bader, G.D. and Hogue, C.W. (2003) An automated method for finding molecular complexes in large protein interaction networks. *BMC Bioinform.*, **4**, 2.